Assessment of Geometric Distortion as part of Quality Assurance in Multicentre Magnetic Resonance Imaging Research

Final Report

December 2012

Dr Jennifer Macfarlane

Lay Summary

Magnetic Resonance Imaging provides superb soft-tissue contrast and flexible imaging making it a versatile modality in a wide variety of diagnoses and fields of research. The introduction of higher magnetic field strengths into clinical use (fields up to 3 Tesla or 3T) permits imaging to be performed faster and/or with greater image resolution. The drawback of higher field strengths is that it is technically difficult to achieve perfectly uniform magnetic fields within the bore of the scanner and this manifests itself as geometric distortions in the images. The precise design of the scanner has a significant impact on the geometric accuracy.

Throughout Scotland there are six 3T MRI scanners of varying design and manufacture. Although acceptance tests have been carried out to ensure that all the scanners are within the agreed manufacturer's specification, research studies involve intricate analysis of images and this could be affected by even small degrees of geometric distortion within each scanner or subtle differences between the degree of distortion seen in different scanners.

The electromagnetic field within an MRI scanner is computed by solving Maxwell's equations and so it is particularly appropriate that funding from the James Clerk Maxwell Foundation has permitted us to measure the geometric distortion of those six scanners.

A large test object was shipped to each of the centres where it was imaged in a similar manner on each of the scanners. The test object was a large, oil-filled 40kg cuboid filled with a series of grids of known geometry. The intersection of the grids provided a very large number of ‘control points’ that could be used to map the geometric accuracy of the images throughout a large volume. A software analyst was employed to create software that would

automatically identify the control points since manual identification is not a practical option. Data has been acquired, collated and analysed.

We found that the manufacturer and design of the scanners has a quantifiable impact on the degree of geometric accuracy. Within the six scanners there are two ‘pairs’. Both Edinburgh and Glasgow have Siemens Verio scanners and Dundee and Glasgow both have Siemens Trio scanners. A very similar performance was seen in both those pairs, making them particularly well-suited to bi-centre studies.

As expected, those scanners with wider and/or shorter bores for patient comfort compromised a degree of geometric accuracy.

In addition to the main static magnetic field, MR scanners rely on magnetic field gradients that are rapidly switched on and off during imaging. Geometric accuracy requires that these behave linearly, but this becomes more challenging when gradient strengths and speeds are increased. Furthermore, the faster and stronger the gradients the more acoustic noise is produced. As a result, manufacturers commonly permit different modes in which the gradients can be applied so that the speed and noise can be adapted to suit the clinical situation. Tests of data acquired in the three modes available on Siemens scanners indicated that they have no impact on the geometric accuracy of the data. When we analysed data from the Philips scanner we saw a subtle difference that would not have been identifiable simply by inspecting images.

Manufacturers provide correction algorithms to improve the geometric accuracy of their data and analysis carried out as part of this study has quantified the impact that they have, showing that the Philips algorithm is particularly effective.

While there remain differences in the geometric accuracy of the six 3T scanners we can now quantify them and allow clinicians and researchers with an interest in areas such as radiotherapy treatment planning, neurosurgical planning or volumetric studies to assess whether they provide data that meets the needs of their application.

MR data can be acquired in a very wide variety of ways to exploit different image contrasts and provide different insights into the structure, physiology and state of internal organs. Each mode of acquisition will have a different impact on the geometric accuracy. Through the JCMF we now have the resource of a filled phantom and analysis software that will allow us to make assessments of new imaging sequences as they are implemented in new studies and applications.

Introduction

The strength of magnetic resonance imaging (MRI) is its excellent soft-tissue contrast and ability to scan in any plane orientation. These advantages offer benefits for the delineation of target volumes for radiotherapy and for many soft tissue sites and cerebral tissue, MR is able to provide enhanced visualisation of lesions over other imaging methods, thereby improving target delineation.

New techniques that image biomarkers of brain tumours such as multi-voxel magnetic resonance spectroscopy (MRS) and diffusion tensor imaging which can detect subtle changes in white matter organisation allow a better delineation of tumours than is possible with conventional imaging techniques. (Price SJ & Gillard JH). The advent of treatment planning based on MR data alone has arrived. (Kapanen M *et al*)

Information about white matter tracts has been used to infer the position of the thalamic nuclei which remain difficult to discern on MR images and has been used in neurosurgical planning for thalamotomies (Kincses *et al*).

The confluence of valuable information from multiple imaging modalities MRI, PET (positron emission tomography) and CT (computed tomography) has a vital role in neurosurgical planning (Risholm *et al*).

In order to have the desired effect and to minimise damage to areas surrounding the target of treatment, information must be obtained with good geometric accuracy.

Furthermore, volumetric assessment of organs or substructures of the brain can be instructive in the development of disease. In 2008 Frisoni *et al* described the changes in hippocampal volumes in Alzheimer's Disease and normal ageing using MRI. Again, a high degree of geometric accuracy is required if reliable patterns are to be established and aid in patient diagnosis and/or treatment monitoring.

Since its introduction into human imaging in the mid 1980s, the operating field strength of MRI scanners has increased from relatively low fields of 0.15Tesla (T) to 1.5T or 3T and up to 7T for research.

Increasing the field strength increases the signal to noise ratio (SNR) of the acquired data which permits the acquisition of data in shorter periods of time, or with increased resolution. It also improves the performance of inherently low SNR techniques such as functional MRI (fMRI) and magnetic resonance spectroscopy (MRS).

The disadvantages of increased field strength are that safety precautions are more stringent and the degree of artefacts present in the data is increased in general. At higher field strengths it is more technically challenging to create a homogeneous static field which results in increased geometric distortions in the image.

The design of MR scanners is driven by a requirement to accommodate people who are claustrophobic or have a large body habitus and as a result, wide bore scanners are being introduced. Widening the bore of the magnet makes it more challenging to achieve a homogeneous static field.

A demand for faster imaging techniques has resulted in faster gradients, but at the expense of linearity.

Reconstruction of MR images relies of the assumptions that there are both a uniform static magnetic field and a perfectly linearly varying gradient field present. Deviation from these assumptions results in an image with a warped geometric representation of the object or subject being scanned.

SINAPSE is a network which operates throughout Scotland providing high quality medical imaging for the research community. It has extensive MRI facilities including 3 Tesla scanners in Dundee, Edinburgh, Aberdeen and Glasgow. When researching conditions with a low prevalence, individual centres can struggle to recruit sufficient participants to their studies from their local populations. Performing multicentre work permits recruitment from a far larger population but carries with it the need to ensure a common standard of performance for the imaging equipment in each site.

The scanners throughout Scotland are manufactured by the three major MR scanner manufacturers. (See Table 1)

Scanner	Location	City	Field Strength (Tesla)	Manufacturer	Model
A	Clinical Research Centre (CRC)	Dundee	3	Siemens	Trio
B	Aberdeen Royal Infirmary	Aberdeen	3	Phillips	Achieva
C	Clinical Research Imaging Centre (CRIC)	Edinburgh	3	Siemens	Verio
D	Institute of Neurological Sciences, Southern General Hospital	Glasgow	3	GE	Signa HD
E	Centre for Cognitive Neuroimaging (CCNi)	Glasgow	3	Siemens	Trio
F	British Heart Foundation Glasgow Cardiovascular Research Centre (BHF GCRC)	Glasgow	3	Siemens	Verio

Table 1 Scottish 3 Tesla MRI scanners involved in the Geometric Distortion comparison.

Geometric distortion is assessed by scanning an object of phantom of known geometry and comparing the spatial co-ordinates of features of the phantom in the image with their real-life counter-parts.

Phantoms vary in their complexity, ability to assess distortion in 1, 2 or 3 dimensions, their sampling density and the volume of assessment.

In 1996 McRobbie described a phantom designed to assess a number of MR image quality parameters. It included 12 rods which permit a 2 dimensional assessment of distortion. In 2004 Janke *et al* increased the sampling density by using a phantom with 68 rods which was imaged in three orthogonal

orientations in order to provide a 3D assessment. Both phantoms were less than 200mm in diameter.

In 1992, Bakker *et al* used a phantom with a diameter of over 30cm to distinguish between static field and gradient errors. A regular grid of 5mm diameter sample tubes filled with $MnCl_2$ solution at 5cm intervals was used.

They comment that the remaining air-filled volume of the phantom could be filled with liquids of different susceptibilities to further investigate the susceptibility-induced geometric distortions.

Within medical imaging, a number of imaging modalities are available, each with their own strengths and weaknesses. In 2003 Karger *et al* created a phantom suitable to compare their geometric accuracies. This was an 18cm diameter phantom that contained five target points and 4 linear rods.

In order to make a 3D assessment of distortion, Schad *et al* made use of two phantoms. The first was a 2D rod phantom which permitted an assessment of the within plane distortion. The second contained rectangularly cross-sectioned rods parallel to the axis of the phantom and circularly cross-sectioned rods oriented obliquely to the axis of the phantom. The distance between squares and circles on the acquired images give an indication of the through-plane distortion.

With a view to assessing accuracy over a wider volume, Tanner *et al* presented a design driven by pelvic radiotherapy treatment planning. The phantom comprised 3 interpenetrating orthogonal arrays of water filled PMMA tubes with exterior dimensions $400x400x250mm^3$. This design has the advantage of being reasonably light however, PMMA is prone to warping with temperature increases and state of hydration. While this phantom provides information about distortion in all three dimensions, it is necessary to look as distortions in different layers displaced from one another. Distortions in x, y and z planes are not readily available for point locations.

There are two designs of phantom that are capable of assessing geometric distortion at individual points in three dimensions using a single image dataset. The first was described by Breeuwer *et al* and involves small spheres mounted on rods and evolved to a design comprising a series of spherical

voids machined into plates of Perspex. A phantom with 427 references points designed to fit into a head coil and one with 793 points for use with a body coil were created. The second involves layers of grids where control points are defined by the corners of the squares of the grids and the interface between the grid and the fluid filling the phantom. This was described by Wang *et al* and provides a higher density of control points than those described by Breeuwer.

With the increasing complexity of phantoms comes a need for software to automatically identify control points within the phantom.

Aims

To compare the level of geometric accuracy of the six 3 Tesla scanners installed in Scotland.

Methods

Phantom

The phantom used in this study was a 3D Geometry Phantom, Model: MRI/3D GRID GEO/REC, manufactured by Wang *et al* to a design similar to that described in their 2004 publication[1].

It comprises a dense 3D array of markers. A series of equally spaced, parallel grid sheets are contained within a box of extermal dimensions $436\text{mm} \times 348\text{mm} \times 248\text{mm}$.

This phantom differs from that described in Wang *et al*[1] in several respects:

- it is larger having dimensions of 436mmx 348mm x 248mm instead of 310mm x 310mm x 310mm.
- as a result, support columns are introduced to lend structural stability.

The consequence of these changes is that our phantom extends to areas of the bore further from the isocentre of the static magnetic field than the original version. Since field heterogeneity becomes significantly more pronounced as

you move from the centre of the scanner, the images become more severely distorted.

This and the presence of columns presented additional challenges to the image analysis program written to analyse the data. As a result it was not possible to directly implement the analysis approach described in Wang *et al*.

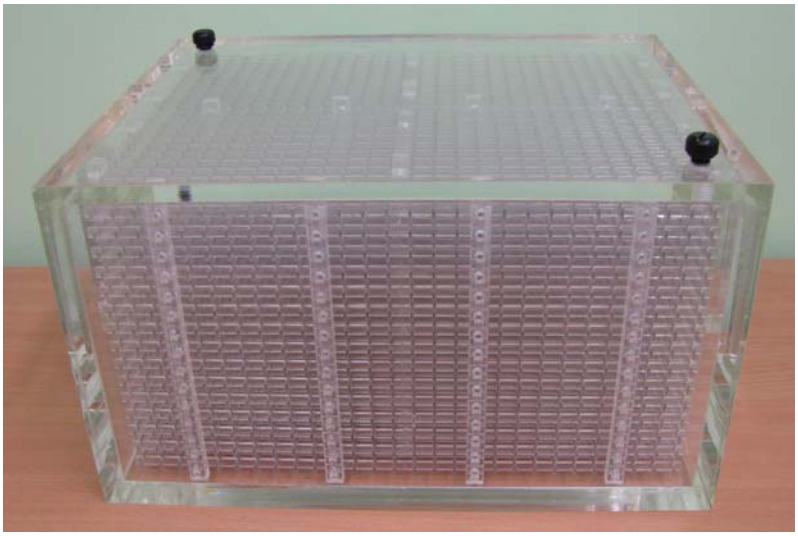

Figure 1 The Geometric Distortion Phantom

The majority of MR phantoms are filled with aqueous solutions of $NiCl_2$, $MnCl_2$ or $CuSO_4$, for use at 1.5 Tesla, however the higher operating frequency of a 3 Tesla scanner can create dielectric resonance effects that create image artefacts. This phantom was therefore filled with Silicon Oil, whose dielectric properties are such that dielectric effects are minimised.

Markers were etched onto the surface of the phantom to allow reproducible positioning of the phantom in different scanners.

The phantom was then scanned in all the scanners shown in Table 1.

Imaging Sequences

MR data can be acquired in a myriad of different ways allowing different image contrasts. The pattern of application of gradient magnetic fields, RF pulses and data acquisition is referred to as an imaging sequence.

To add a further layer of complexity, manufacturers implement imaging sequences in subtly different ways and give them different names.

It is not therefore possible to acquire the data in exactly the same manner from all the different scanners.

- a sequence that is closely matched to one used Wang *et al*.
- a spin echo sequence – a simple sequence that should not differ significantly in its implementation between manufacturers and
- a high-resolution sequence used for geometrically critical imaging with the caveat that the imaging field of view had to be scaled up to include the whole volume of the scanner in the imaging volume.

Data has been acquired with and without manufacturer provided geometric distortion corrections where possible.

It was possible to use exactly the same sequences for the four Siemens scanners.

CT acquisition

A CT image data set was acquired using a Siemens PET/CT Biograph mCT. CT data is known to be distortion free and acts as a gold standard (Baldwin *et al*, Yu *et al*, Doran *et al*, Karger *et al* 2006). While a description of the geometry of the phantom was provided by the manufacturer, CT data permits the verification of the geometry of this particular phantom, including any manufacturing or structural variances.

Analysis Software

A software programmer was employed on a temporary contract to create custom software using Matlab to automatically identify the control points within the phantom, summarise and quantify the level of geometric distortion present.

The programme employs an approach similar to that described by Wang and colleagues. (Wang *et al* 2004). There are two stages to target point identification. This first is an initial identification of the control points, followed by a sub-pixel localisation.

This initial identification is performed on a first derivative of the data which highlights changes in image intensity and therefore boundaries between the silicon oil and the Perspex grids. The process is semi-automated. The user is required to select a starting point and definite its co-ordinate within the phantom. The program searches a small volume around the start point for an intensity maxima to find the first initial control point. From those co-ordinate it shifts a distance determined by the actual geometry of the phantom along each of the co-ordinates, creates another volume around that point and searches for the next local maxima. By incrementing through the x,y and z co-ordinates an initial estimate of the position of all control points is estimated. This process is depicted in Figure 2.

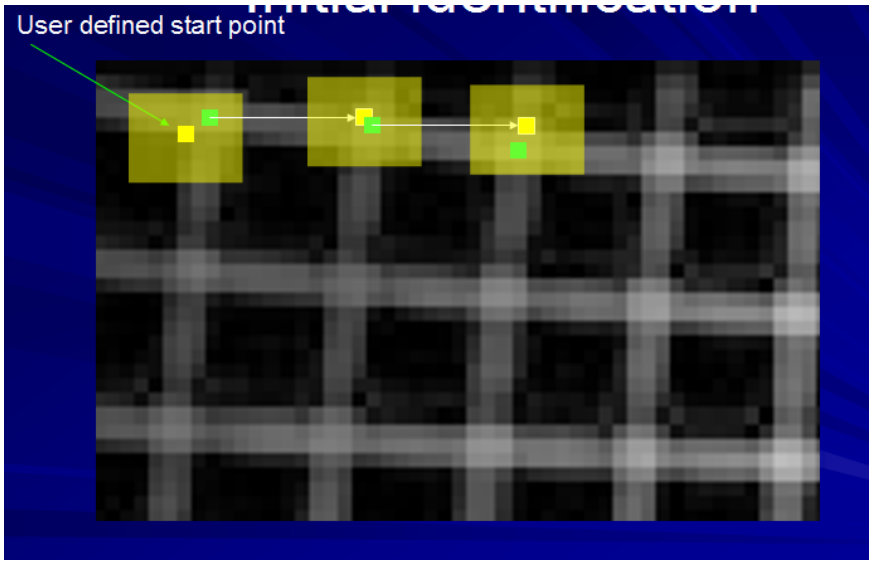

Figure 2. The leftmost yellow dot shows the user-defined start point. The transparent yellow box indicates the search volume for the local maxima, shown by the green dot. From here, the position of the next expected control point is calculated (shown by the middle yellow dot). The process of searching a volume for the local maximum is repeated. This process is continued in the x,y and z directions.

In the second stage of the analysis, each co-ordinate it refined by taking the first derivative in the x, y or z direction and performing a centre of mass calculation to a sampling volume about the initial x, y or z co-ordinate, permitting sub-pixel localisation.

The co-ordinates of the MRI control points and then compared with those found by a similar method from the CT dataset and the difference in positions are calculated in the x, y and z direction as well as in absolute dimensions.

Results

The phantom has been scanned in all six 3 Tesla scanners. Below are two examples of images that demonstrate the geometric distortion without the application of the manufacturer's distortion correction. Figure 3 shows an image of the data acquired from the a Siemens Trio scanner. The imaging sequence acquired data from the whole of the phantom volume. Coronal, sagittal and axial cross-sectional slices are shown. The coronal plane shows the pattern of the grid sheets used in construction. The small squares at the periphery and through the centre of the phantoms are the support pillars. The sagittal and axial slices are taken from the centre of the phantom and so the thick horizontal and vertical bands are the support columns once more. Figure 3b presents the same data, but the sagittal and axial slices are taken from slightly off-centre positions to avoid the support structures.

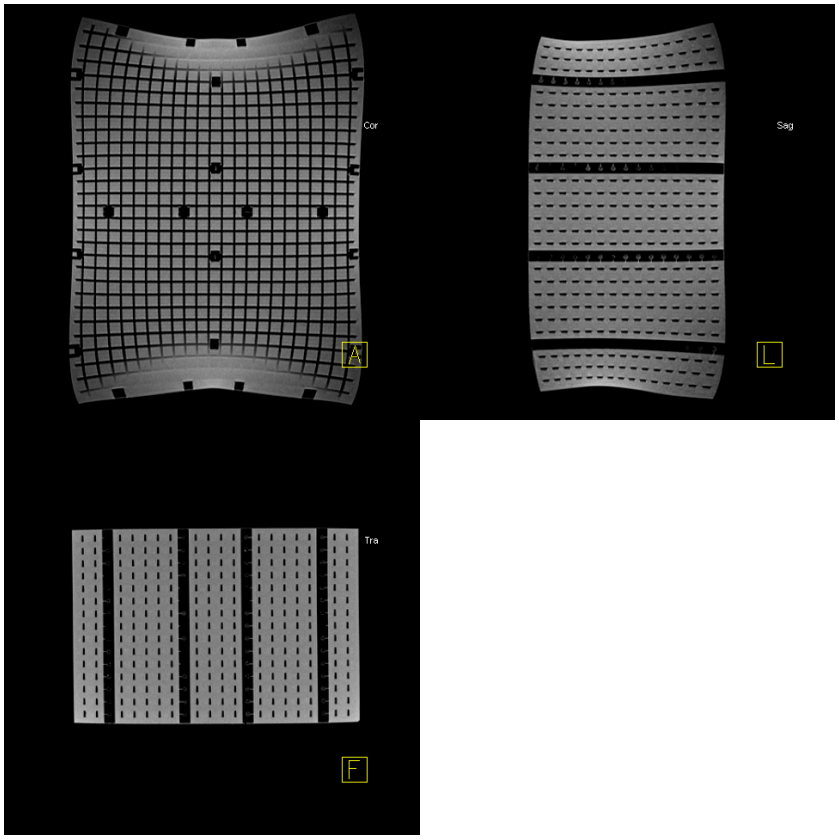

Figure 3a Data from a Siemens Trio scanner. Transverse and Sagittal slices take through centre of Coronal slice and therefore show the support columns.

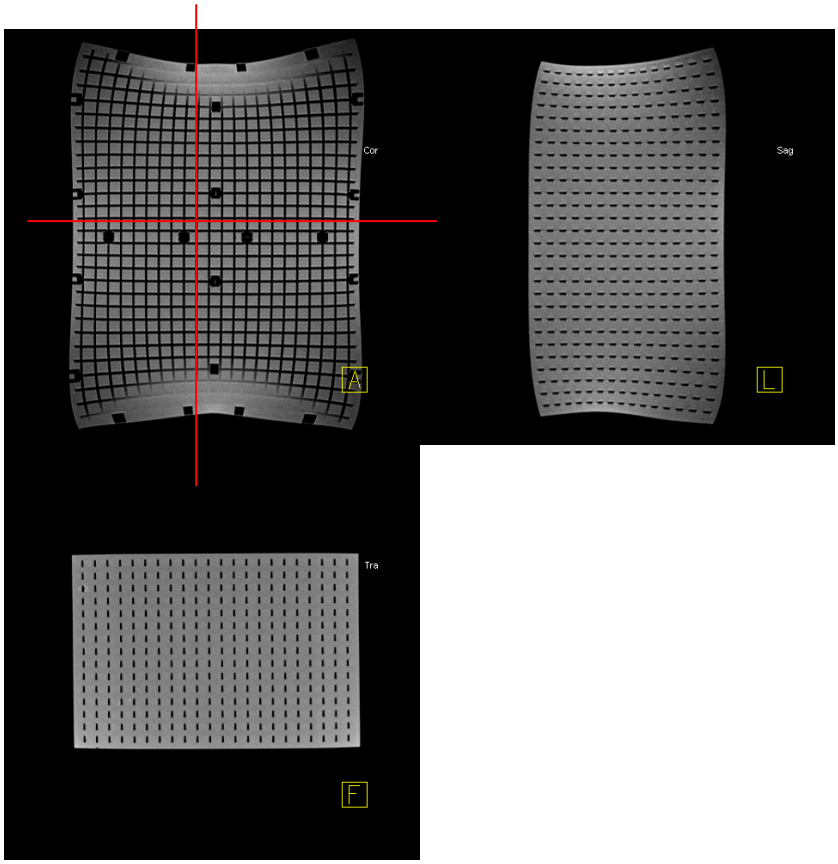

Figure 3b The same Siemens Trio data. Transverse and Sagittal slices taken off-centre through Coronal slice (avoiding pillars). Slice position is shown by the red lines.

A brief inspection of these images confirms that we do not have true mapping of the geometry of the rectangular phantom. We see a bowing of the structure that becomes progressively worse, as we move further from the centre of the phantom and the centre of the scanner (or isocentre).

Figure 4 shows data from the a Siemens Verio, using the same format of data slices as used in Figure 3b. this data was acquired with the same imaging sequence as that employed for the data shown in Figure 3. The pattern of distortion is noticeably different and more severe. This is to be expected since the Verio is a wide bore scanner whereas the Trio is not. It is more challenging to create a homogeneous static magnetic field in a wide bore scanner and this is clearly reflected in these images.

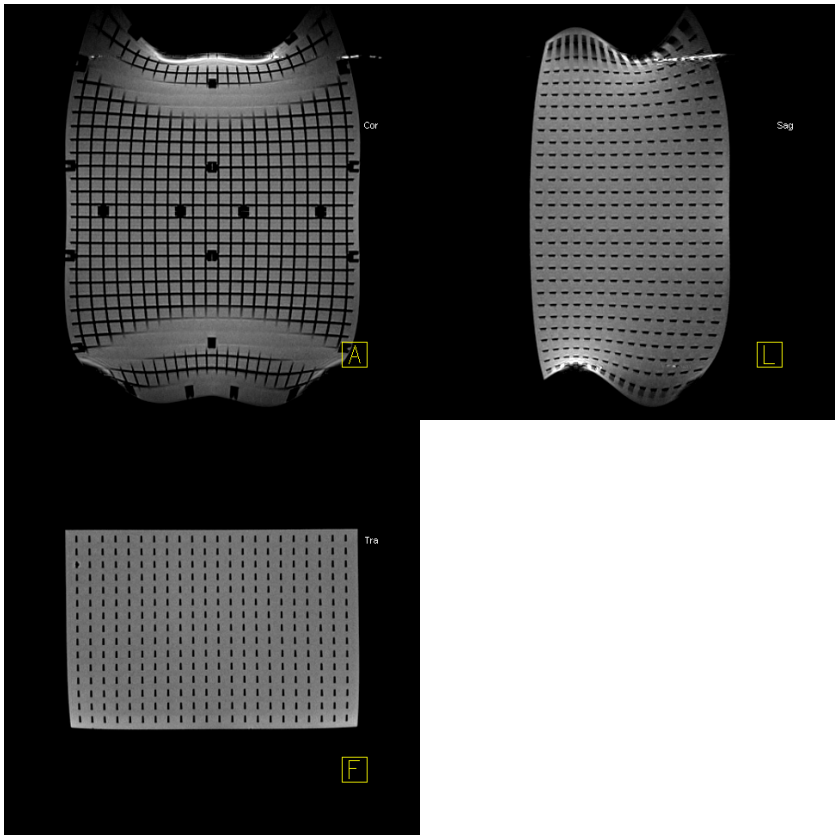

Figure 4. Siemens Verio data. Transverse and Sagittal slices taken off-centre through Coronal slice (avoiding pillars).

Manually identifiying all the control points or intersections of the phantom in the acquired images would be a painstaking task. Software was therefore written in Matlab to allow the automatic identification of the control points, perform a comparison with co-ordinates obtained from CT data and present the results in an accessible manner. The output of the Matlab software is shown in Figure 5.

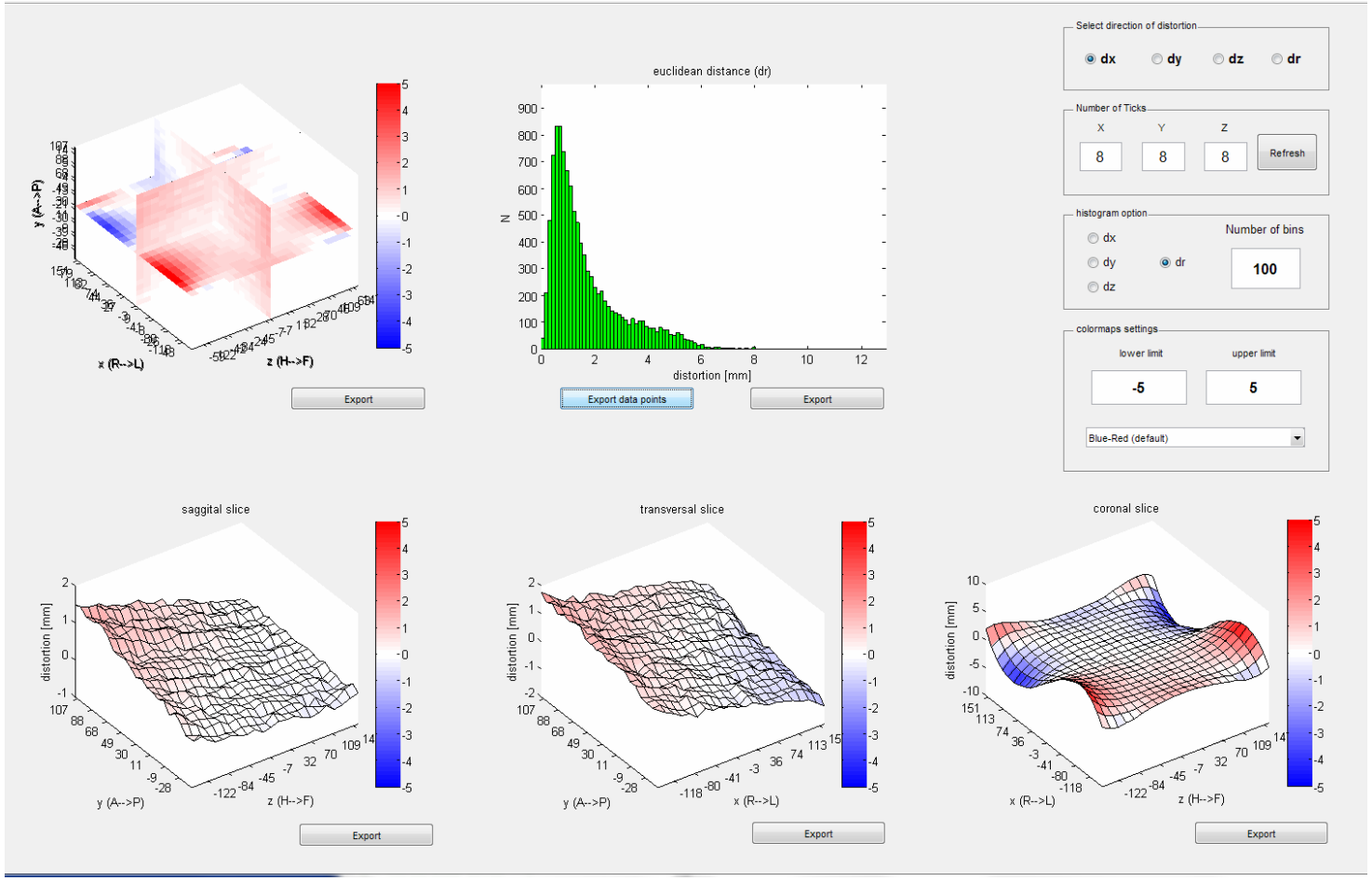

Figure 5 An example of the geometric distortion results display.

This GUI plots the geometric distortions in a number of formats:

The top left plot shows the distortion as a 3D chart. By clicking and dragging each of the slices, they can be scrolled through all three dimensions. The corresponding distortions will be shown in the bottom three plots as surface plots. The direction of the distortions (in the x, y or z direction (dx, dy or dz) or as an absolute distance (dr). This is particularly useful for developing an understanding of how geometric accuracy varies throughout the imaged volume.

The histogram in the centre of the top row shows how frequently a distortion of a particular size is found and is useful as on overview of a whole image volume. Again, this can be plotted in terms of dx, dy, dz or dr.

A facility to export data was included to permit data from different datasets to be overlaid for comparison.

The program is robust for large volumes of the phantom, but the detection algorithm struggles when distortion is particularly large at the extremes of the geometry of the phantom. It is therefore equipped with the ability to analyse a subset of the phantom volume.

Relationship between the distance from isocentre and distortion.

Figures 3 and 4 demonstrate qualitatively that distortion is more pronounced as the position within the phantom moves further away from the isocentre of the scanner.

This relationship can be inspected more closely using the custom-written software, as shown in Figure 6.

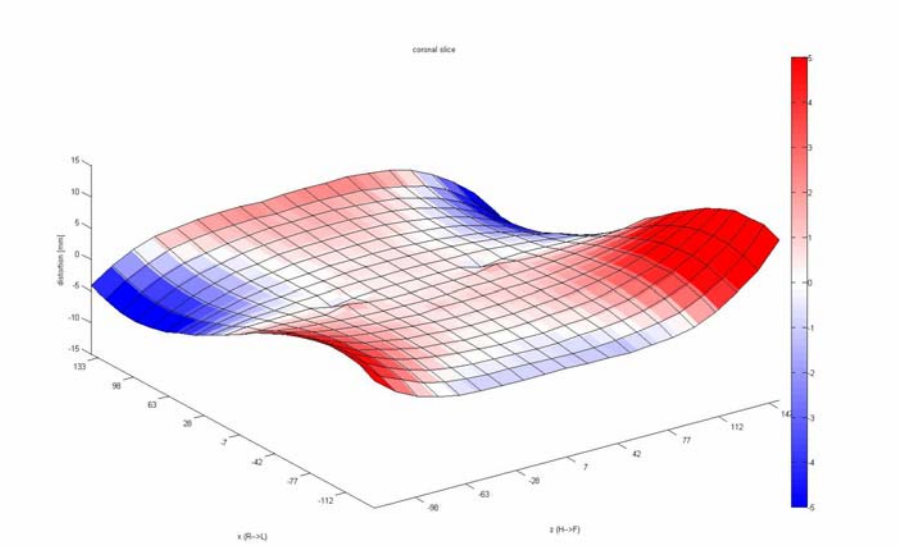

Figure 6 This shows the geometric distortions in the x-direction (right to left for a 'patient' lying head-first, supine in the scanner), in a central sagittal plane. This is data from a Siemens Verio and distortions have been calculated over a volume of 266 x 266 x 133mm^3.

This shows that distortions become greater as you move away from the centre of the phantom and the isocentre of the magnet.

This pattern was quantified by looking at different sub-volumes of the phantom. Each one was centred on the middle of the phantom and they were (10 x 10 x 10), (16 x 16 x 16) and (20 x 20 x 20) control points. This corresponds to volumes of (126 x 126 x 63) mm^3, (210 x 210 x 105) mm^3 and (266 x 266 x 133) mm^3. The plot shown in Figure 7 plots the percentage of points that have a distortion of a given size or less. For example: when considering the smallest central volume, the percentage of points with a distortion of 1mm or less is 96%. This falls to 71% and 50% for the (16 x 16 x 16) and (20 x 20 x 20) volumes, respectively.

This analysis was repeated with data a Siemens Verio and the corresponding values for the percentage of control points with a geometric distortion of 1mm or less was 80%, 38% and 21% for volumes of (10 x 10x 10), (16x16x16) and (20x20x20) control points, respectively. This is shown in Figure 8.

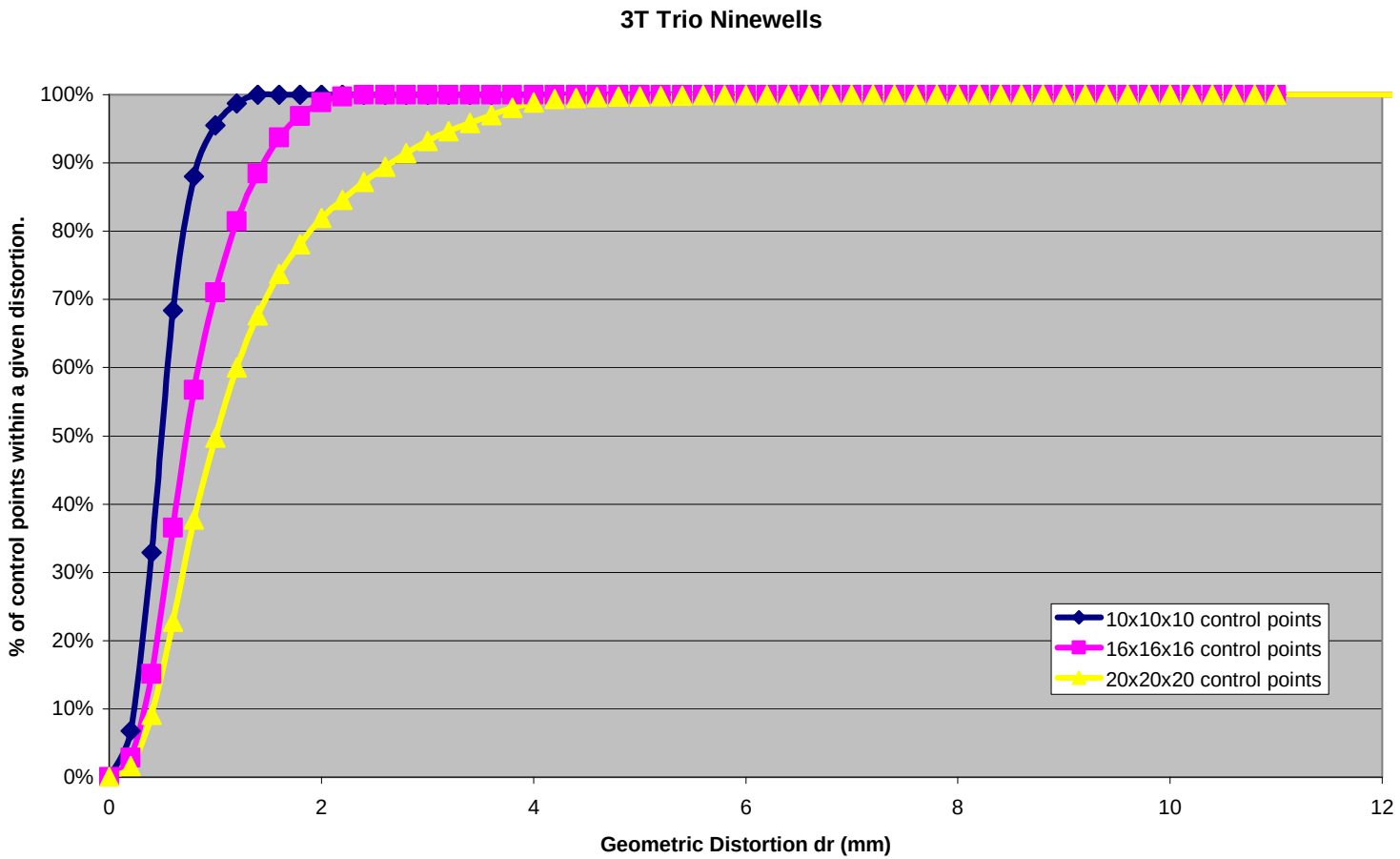

Figure 7.A cumulative plot of the percentage of control points with a given geometric distortion (dr in mm) or less. Data acquired from a Siemens 3T Trio and analysed over three central volumes.

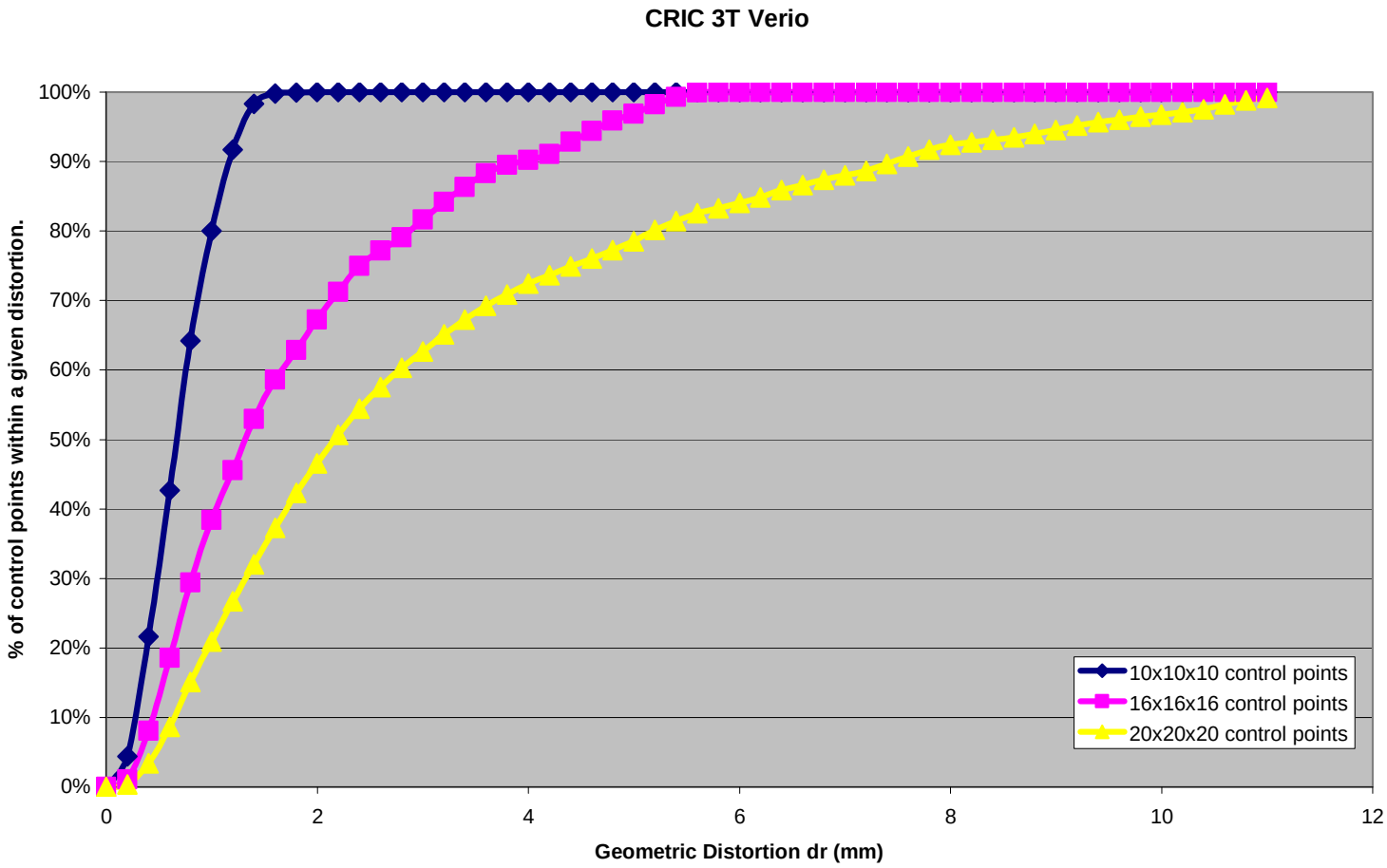

Figure 8 A cumulative plot of the percentage of control points with a given geometric distortion (dr in mm) or less. Data acquired from the a Siemens Verio and analysed over three central volumes..

Geometric Distortion comparison of six scanners.

Figure 9 shows the range of distortions seen in a (20 x 20 x 20) central control point volume (or a 266 x 266 x133 mm^3 volume) for all six scanners.

Table 2 shows summary values for the absolute distortion (dr)

Scanner	A	B	C	D	E	F
Mean ± st dev (mm)	1.28±0.91	2.68±2.32	3.14±2.69	2.78±1.58	1.42±0.95	3.16±2.69
Max (mm)	7.04	10.88	12.06	10.38	7.49	12.50

Table 2. Absolute Geometric Distortion (dr) values for three scanners, assessed over a volume of 266 x 266 x 133mm^3. For scanners A C E and F, these figures are based on 3D - vibe acquisitions. For scanner B, a 3D-T1 weighted image was used while data was calculated from a 3D IR-FSPGR with grad warp applied. No geometric distortion correction was applied to data from scanners A,B,C, E or F.

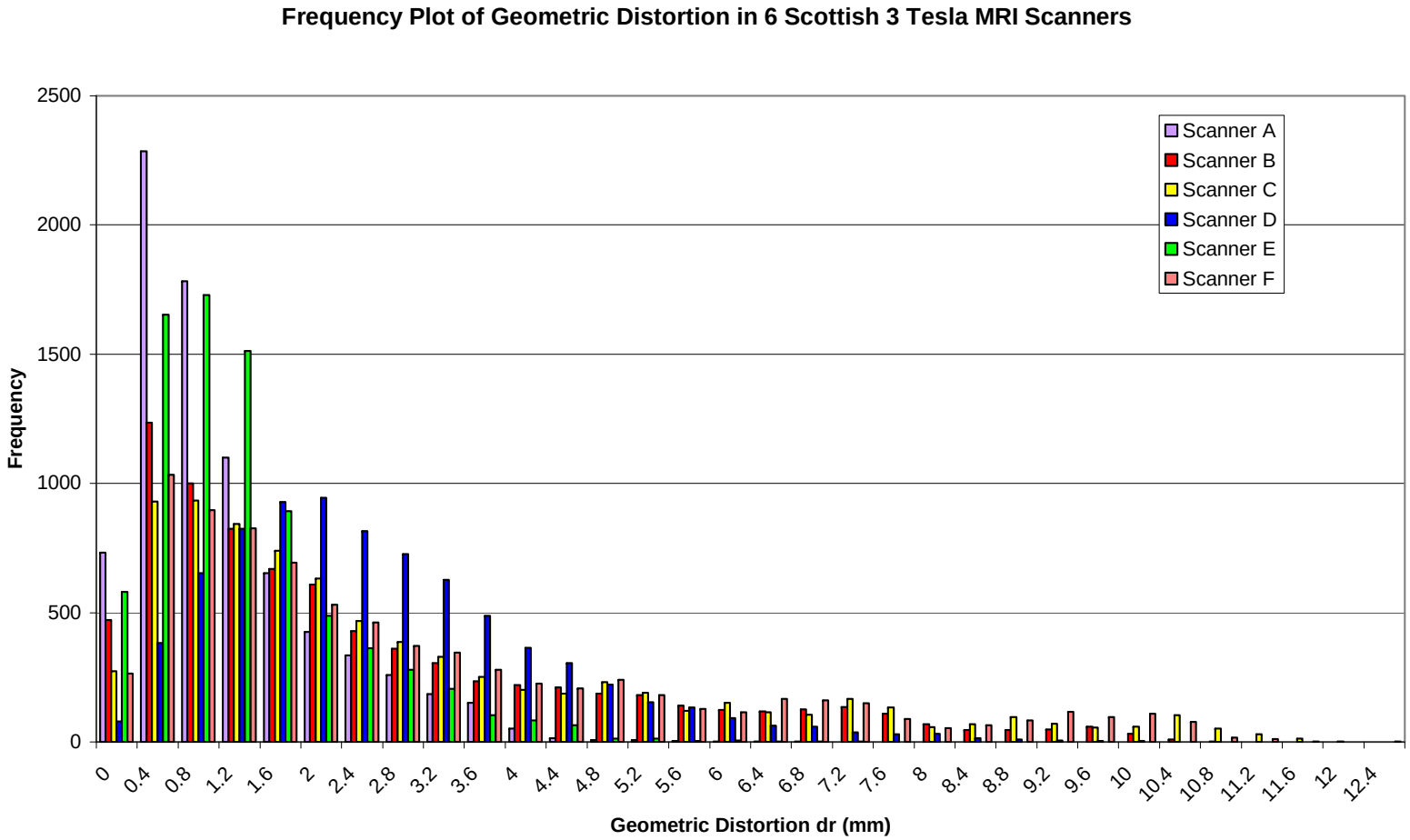

Figure 9 Frequency plot of Geometric Distortion over a volume of 266mm x 266mm x 133mm for 6 scanners

Table 2 and Figure 9 indicate a variation in performance. This can be related back to the design and purpose of the scanners themselves.

Scanners C and F are Siemens Verio scanners which have a 70cm bore – 10cm larger than all the other scanners. Coupled with a short magnet length, this results in a greater degree of distortion.

Scanner D is a GE scanner which is dedicated to neuroimaging and is optimised for imaging smaller volumes than the other scanners which are all used to image other, generally larger regions of the body. It has a comparatively short bore length which is reflected in the distortion figures.

Scanners A and E are Siemens Trios and show very similar distortion profiles, as expected.

Comparison of gradient modes

Some scanners can be run in different gradient modes, permitting either faster imaging (fast mode) or slower, but quieter imaging for patients or volunteers who may be anxious about the scanning procedure.

Images were acquired in the three modes available on Siemens scanners: whisper, normal and fast. The modes on the Philips scanner are termed maximum, enhanced and default. When imaging with a body coil, it is not possible to change the gradient mode on the GE scanner.

Figure 10 below displays data from a Siemens Trio and shows that the choice of imaging mode has no significant effect on the pattern of distortion. A volume of 22 x 26 x 28 control points was used in this case.

This trend was seen in all the Siemens scanners.

Interestingly, however, there seems to be subtle difference in the distortion seen with different modes in for the Philips data, which is demonstrated in Figure 11. It is not possible to identify this difference by inspection.

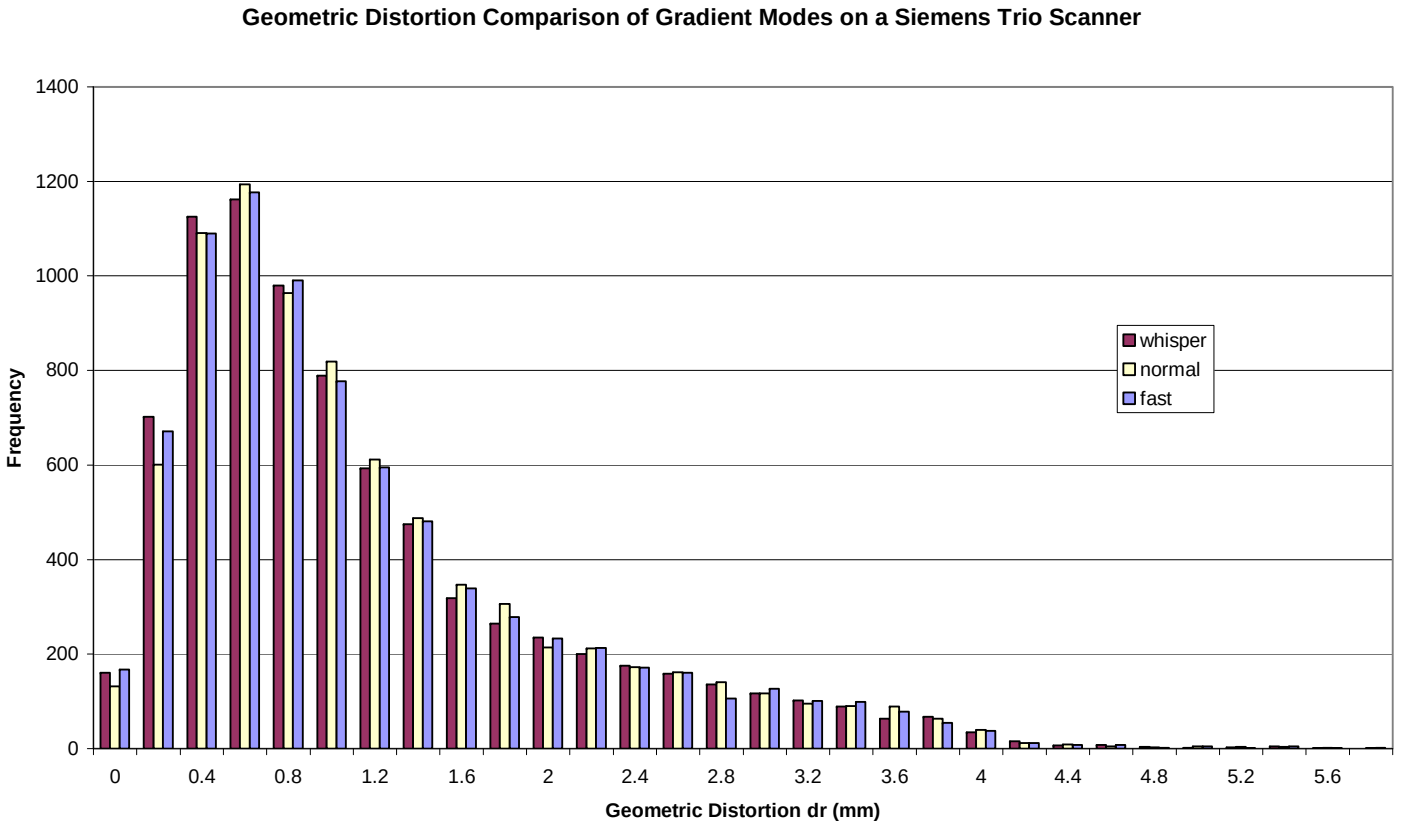

Figure 10 A Comparison of the geometric distortion seen when different gradient modes are employed during a Vibe acquisition on a Siemens Trio.

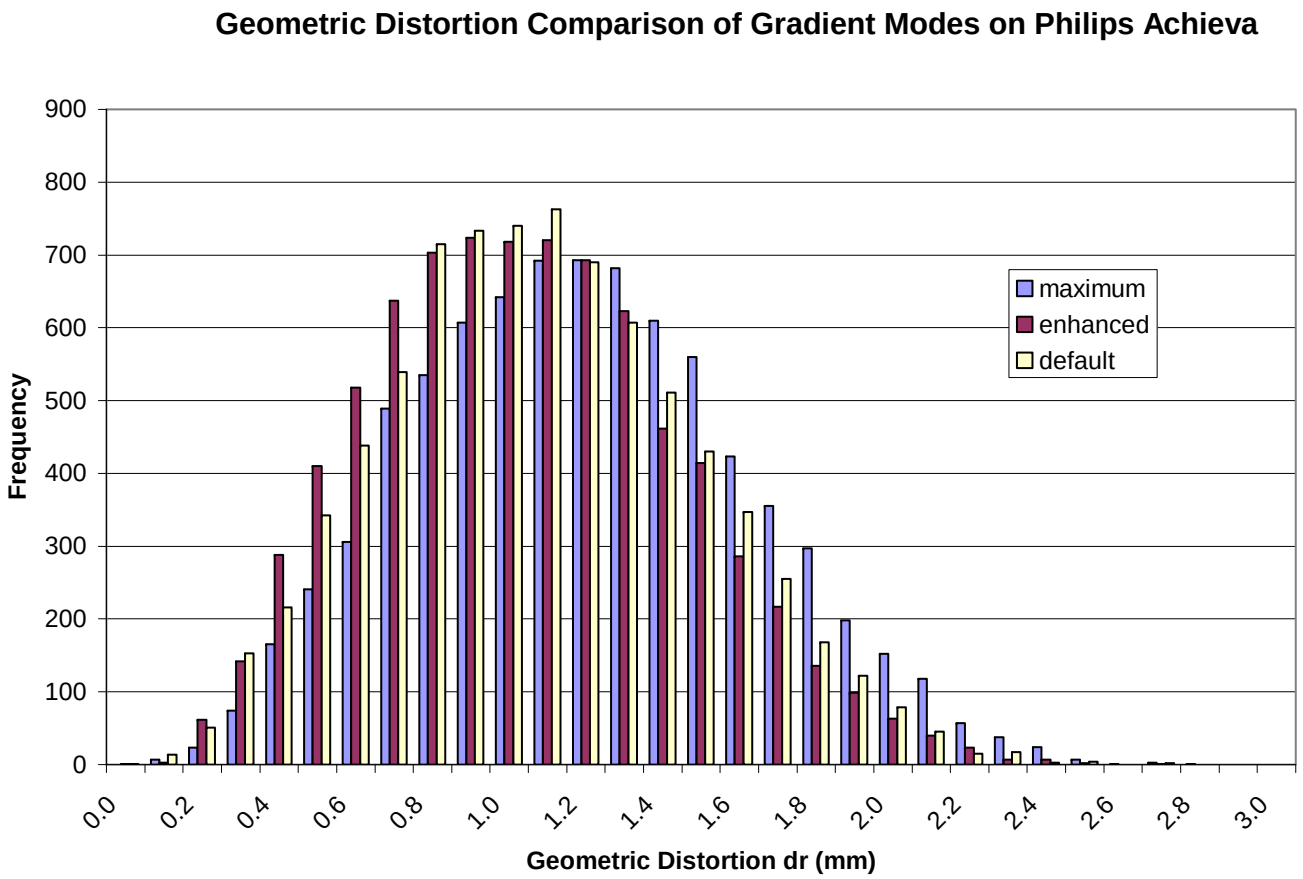

Figure 11 A Comparison of the Geometric Distortion seen when different gradient modes are employed during a T1 acquisition on the Philips Achieva.

Comparison of Different Imaging Sequences

Data acquired from the CRC 3T Trio using two different sequences – a 3d vibe sequence which is closely matched to the sequence used in Wang *et al* 2004 and an MPRAGE which is adapted from a sequence used locally for high resolution imaging where geometric accuracy is of high importance. Figure 12 below shows that there is no significant impact on geometric distortion due to the implementation of the different imaging sequences on this scanner. Distortions were assessed over a volume of 266 x 266 x 133mm^3.

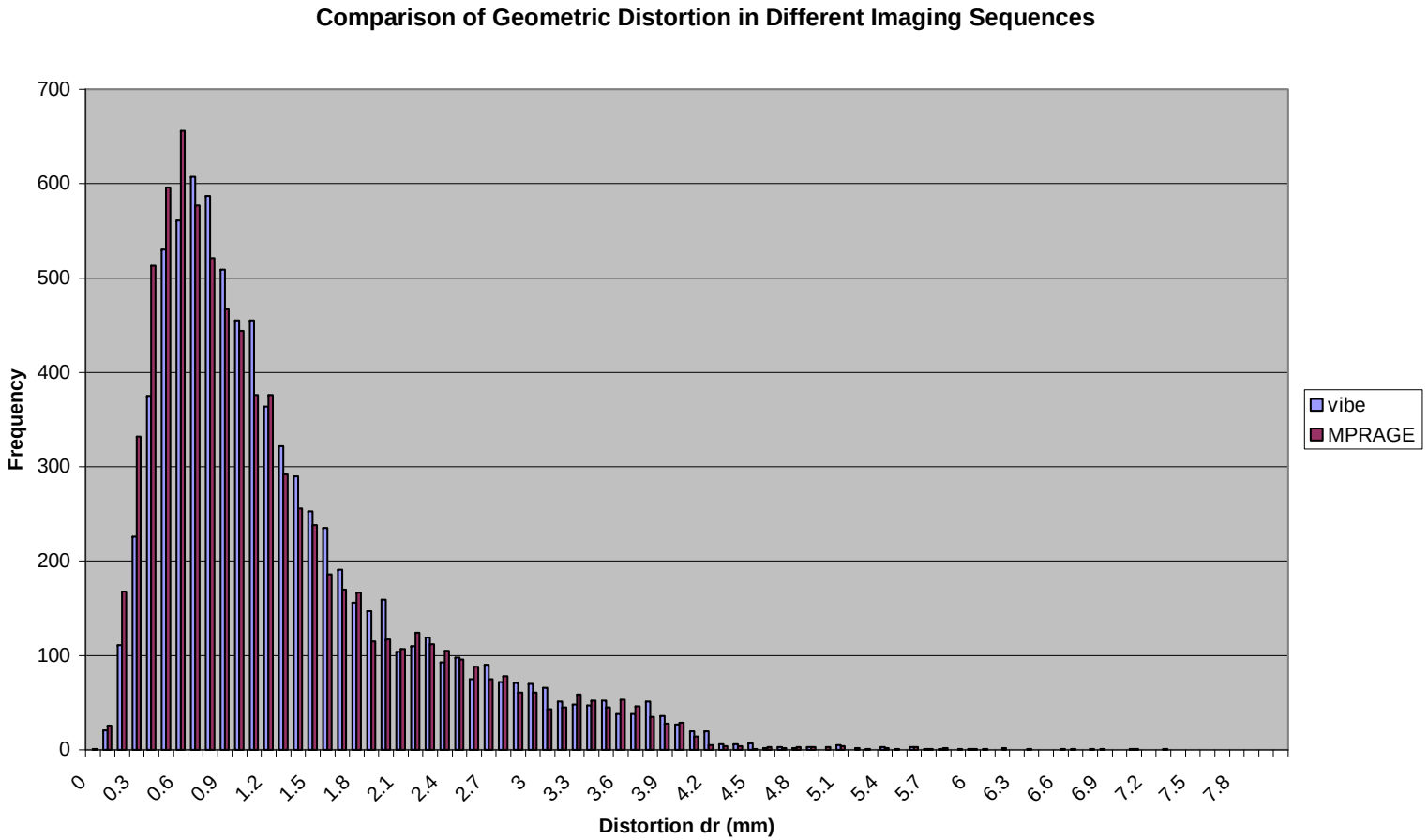

Figure 12 A Comparison of the Geometric Distortion seen in two different acquisition sequences, a vibe and an MPRAGE on the Siemens Trio.

Manufacturer Provided Geometric Distortion Correction Algorithms

The three manufacturers take different approaches to distortion correction algorithms. GE provide a correction referred to as ‘gradwarp’ to account for the short bore length. This is applied to all their data including that presented in Figure 9 (Scanner D). It was not possible to obtain ‘uncorrected’ data. Siemens and Philips provide an algorithm that can be applied as required.

Figure 13 overleaf illustrates the effect of the manufacturer’s geometric distortion correction algorithms.

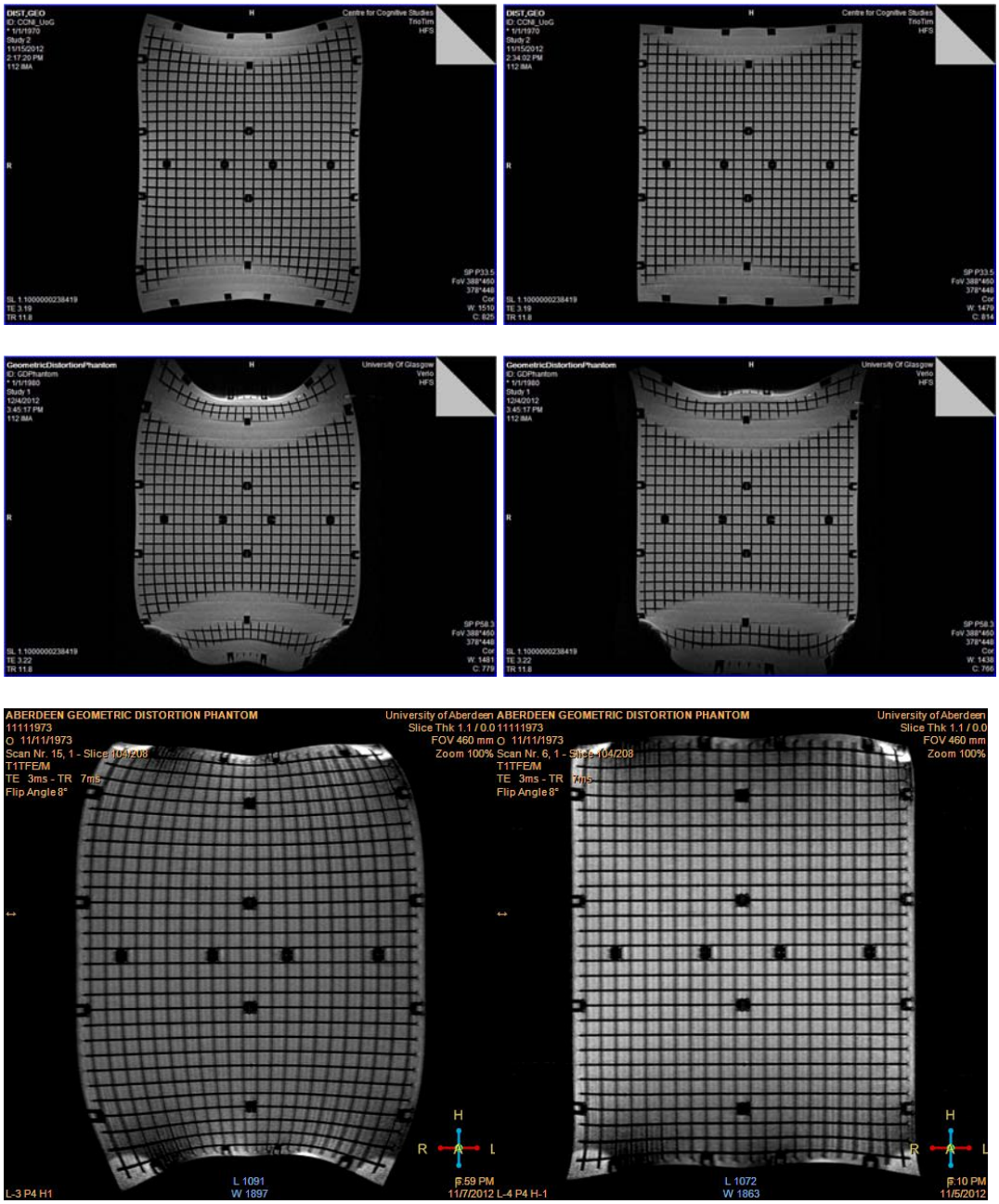

Figure 13 Images showing the effects of applying the manufacturer's distortion correction algorithm. Each image shows a central slice through the phantom. Data in the left had column has not been corrected. The correction algorithm has been applied to the data in the right hand column. The top row illustrate the effect of distortion correction on data from Siemens Trio scanners. The middle row on Siemens wide-bore Verio scanner and the bottom row on data from a Philips Achieva.

The relative effect of the distortion correction algorithms can be seen in figure 14.

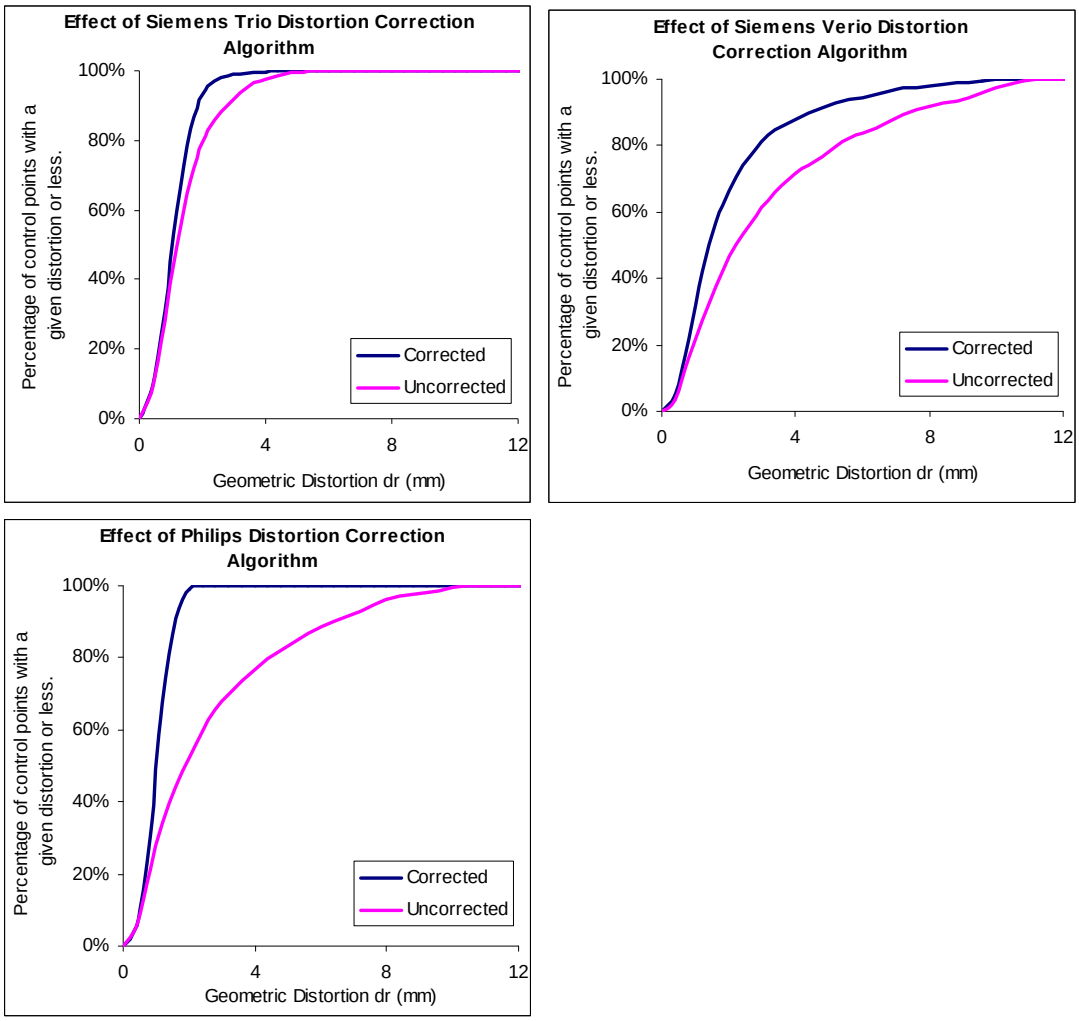

Figure 14 This shows the effect of the manufacturers geometric distortion correction algorithm on data from a Siemens Trio (top left), a Siemens Verio (top right) and a Philips Achieva (bottom).

From these plots and Figure 13 we can see that the correction algorithms have a significant impact on the data. Figure 14 indicates that the Philips algorithm has the most dramatic effect taking the percentage of points with a distortion of 2mm or less from 44% to 99%. On the Siemens Trio scanner this was 80% to 93% and on the Verio 46% to 67%.

Figure 15 indicates the relative performance of data from the three manufacturers after a correction has been applied. The effects of the GE Signa HD's short bore and the Siemen's Verio's wide diameter, short length

bore remain after distortion correction. Data from a volume of 266 x 266 x 133mm^3 was assessed.

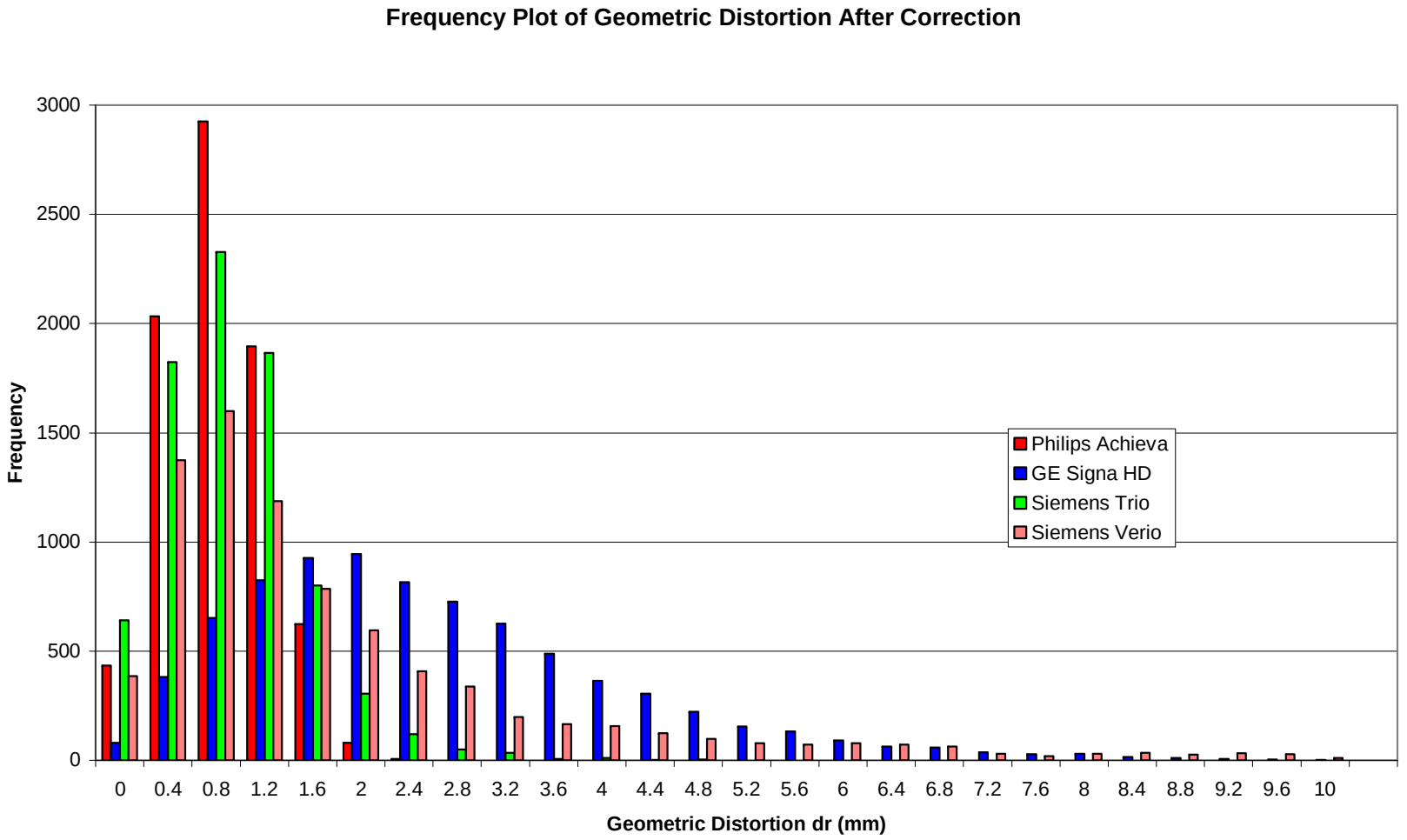

Figure 15 Shows the relative performance of corrected data from three manufacturers and four models of scanner.

Conclusions

As expected and widely reported (for example Baldwin *et al* 2009) the level of geometric distortion increases with the distance from the isocentre of the magnet.

The data acquired in this study does not suggest a strong impact on geometric distortion as a result of using different gradient modes, however the analysis software has allowed the quantification subtle changes as was seen with the Philips data.

The two Siemens Trio scanners in Dundee and Glasgow display very similar distortion characteristics, as do the two Siemens Verios in Edinburgh and Glasgow, as expected.

Before the application of a distortion correction, the Siemens Trio data displayed the smallest amount of distortion, with the wide bore Siemens Verios showing the greatest.

After correction, the Philips Achieva produced the most geometrically accurate data.

The wide bore design of the 3T Siemens Verio explains the increased distortions seen in its data. The 3T GE Signa HD is a few years older than some of the other scanners, has been optimised for brain imaging and has a short length bore which may explain why the static field homogeneity and/or gradient linearity do not perform as well over a large field of view. In light of the data presented here, it may be worth investigating whether GE can provide an update to their ‘gradwarp’ correction or apply a post-acquisition distortion correction.

Other authors have reported maximum distortions over similar (but not identical) imaging volumes of: 10-25mm at 1.5T (Wang *et al*), 9mm at 1.5T (Doran *et al*), 7mm at 3T (Baldwin *et al* 2007).

We have observed maximum distortions of 7 to 12mm. This is not dissimilar to Doran’s results from a 1.5T scanner. The 3T Siemens Trio and the Philips

Achieva compare well with Baldwin’s data which was also acquired from a 3T Philips scanner.

Discussion

The data acquired and presented in this document provide a baseline comparison of the relative performances of six 3 Tesla scanners.

While the results of Figure 12 suggest that the application of two different T1 weighted imaging sequences does not have a significant impact on the degree of distortion seen in the images, this does not reflect the wide range of imaging sequences used in practise. T2 weighted imaging and advanced imaging techniques such as diffusion tensor imaging and functional magnetic resonance imaging are likely to have a different distortion profile. Any multicentre study with a heavy dependence on geometric accuracy should be preceded by an assessment with the phantom using the sequences that are planned for image acquisition in order to assess relative accuracy over a given volume of interest.

The phantom and the software written to analyse the images are particularly useful resources that can be utilised in future and used to assess the efficacy of new distortion correction algorithms whether they are provided by a manufacturer or custom-written.

The degree of error that is acceptable in geometrically critical applications varies from application to application. With the data gathered in this study in conjunction with access to the phantom and analysis program, we can quantify the errors over different imaging volumes to allow informed judgements to made about whether MR data can be relied upon in radiotherapy treatment planning, neurosurgical planning or in volumetric studies.

Further work:

In future this work could be extended to refine software analysis program to investigate whether it is possible to identify control points at extremes of the volume in heavily distorted datasets. This may be achieved by working with other centres within the UK who have written their own custom software to identify control points within the phantom.

Dissemination

This project has been presented at SINAPSE ASMs and the Institute of Physics and Engineering in Medicine’s Magnetic Resonance Special Interest Group Meeting.

Acknowledgements

Thanks go to

James Clerk Maxwell Foundation

Dr John McLean, Institute of Neurological Sciences, Southern General Hospital, Glasgow

Dr Gordon Waiter, Aberdeen Biomedical Imaging Centre, Foresterhill, Aberdeen.

Mrs Frances Crabbe, CCNi, Psychology Building, University of Glasgow, Glasgow

Dr Scott Semple, Clinical Research Imaging Centre, Edinburgh.

Ms Christie McComb, Western Infirmary General, Glasgow.

Marko Erdtel, software programmer.

Dr Janet de Wilde, formerly of SINAPSE.

References

1. Price SJ & Gillard JH Imaging biomarkers or brain tumour margin and tumour invasion. British Journal of Radiology 84 (4) S159-67. 2011
2. Kapanen M. *et al* Commissioning of MRI-only based treatment planning procedure for external beam radiotherapy of prostate. Magnetic Resonance in Medicine 2012 August (Epublication ahead of print).
3. Kincses Z T *et al* Target Identification for Stereotactic Thalamotomy Using Diffusion Tractography. PLoS One 7(1) e29969. 2012.
4. Risholm P., Golby A.J., Wells III W.M. Multi-Modal Image Registration for Pre-Operative planning and Image Guided Neurosurgical Procedures. Neurosurgical Clinics of North America 22(2):197-206 2011.
5. Frisoni GB *et al* Mapping local hippocampal changes in Alzheimer's Disease and normal ageing with MRI at 3 Tesla. Brain 131:3266-3276 2008.
6. McRobbie D A three-dimensional volumetric test object for geometry evaluation in magnetic resonance imaging. Med. Phys. 24(5):737-742 1997
7. Janke A *et al* Use of Spherical Harmonic Deconvolution Methods to Compensate for Nonlinear Gradient Effects on MRI Images MRM 52:115-122 2004.
8. Bakker *et al* Analysis fo Machine-Deopendent and Object-Induced Geometric Distortion in 2DFT MR Imaging MRI 10:597-608 1992
9. Karger CP *et al* Stereotactic imaging for radiotherapy: accuracy of CT, MRI, PET and SPECT Phys Med Biol 48:211-221 2003
10. Schad LR *et al* Correction of Spatial Distortion in Magnetic Resonance Angiography for Radiosurgical Treatment Planning of Cerebral Arteriovenous Malformations MRI 10:609-621 1992

11. Tanner SF *et al* Radiotherapy planning of the pelvis using distortion corrected MR images: the removal of system distortions Phys Med Biol 45:2117-2132 2000

12. Breeuwer *et al* Detection and correction of geometric distortion in 3D MR images Proc SPIE 4322:1110-1120 2001

13. Wang, DM; Doddrell, DM; Cowin, G,A novel phantom and method for comprehensive 3-dimensional measurement and correction of geometric distortion in magnetic resonance imaging MAGNETIC RESONANCE IMAGING Volume: 22 Issue: 4 Pages: 529-542 2004

14. Baldwin LN, Wachowicz K., Thomas SD., Rivest R., Gino Fallone B. Characterization, prediction and correction of geometric distortion in 3 T MR images. Medical Physics 34(2):388-399. 2007.

15. Yu C., Apuzzo M.L.J., Zee C-S., Petrovich Z. A Phantom Study of the Geometric Accuracy of Computed Tomographics and Magnetic Resonance Imaging Stereotactic Localization with the Leksell Stereotactic System. Neurosurgery 48:1092-1099. 2001.

16. Doran S.J., Charles-Edwards L., Reinsberg S.A.m Keach M.O. A complete distortion correction for MR images: I. Gradient warp correction. Phys. Med. Biol 50:1345-1361 2005.

17. Karger C P Hoss A, Bendl R Canda V Schad V Accuracy of device specific 2D and 3D image distortion correction algorithms for magnetic resonance imaging of the head provided by a manufacturer. Physics in Medicine and Biology 51:N253-N261 2006.

18. Baldwin *et al* A two-step scheme for distortion rectification of magnetic resonance images. Med Phys 36(9) 3917-3926 2009